Effect of process conditions on the abrasion resistance of broadband AR films prepared by electron-beam evaporation

Hua Shen (沈 华)[1], Rihong Zhu (朱日宏)[1*], Qing Wang (王 青)[1], and Linhua Xu (徐林华)[2]

[1] *School of Electronic Engineering and Photo-electric Technology, Nanjing University of Science and Technology, Nanjing 210094, China*

[2] *School of Science, Nanjing University of Science and Technology, Nanjing 210094, China*

[*] *E-mail: edward_bayun@163.com*

Received November 25, 2009

Until now, there are few reports on the effect of process conditions on abrasion resistance, which is the most important mechanical property of optical films. Broadband antireflective (AR) films composed of $SiO_2$and TiO_2, whose bands are from 620 to 860 nm and whose reflectivity is less than 0.5%, are prepared by electron-beam evaporation (EBE) at different temperatures, ion beam energies, and cooldown times. The structural properties of the films are investigated by atomic force microscopy, including the surface roughness, crystallinity, shape, uniformity, and compactness of the grain. The abrasion resistance of the samples is tested according to MIL-C-48497A4.5.5.1 standard. We discuss the relationship between abrasion resistance and the structural properties produced under different process conditions, such as preparation temperature, energy of the ion beam, and cooldown time. Grain shape and surface roughness are indicated to codetermine the abrasion resistance of the film. Further, the AR film with triangular grain and moderate roughness shows good abrasion resistance.

OCIS codes: 240.0310.

doi: 10.3788/COL201008S1.0078.

Antireflective (AR) films are used mostly in all kinds of optical films, especially the broadband AR film, which is the most important because transmissive optical components are in great demand. With the advent of optical high technology, which is evident in inertial confinement fusion and the development of the huge astronomical telescope, as well as the need to satisfy the stringent demands of using the optical system for a long time in the field, it is necessary to pay attention to enhancing the mechanical properties of films, including abrasion resistance. In recent years, many scholars have researched on the improvement of the abrasion resistance of films[1−10]. However, most papers focused on superhard films such as TiN and TiC[1,2] or on the improvement of preparation methods to obtain single-layer films with high abrasion resistance, such as ZrO_2[3,4], TiO_2[5], and MgF_2[6].

At present, there are several methods to prepare broadband AR films, such as the electron-beam evaporation (EBE) method, radio-frequency magnetron sputtering, and sol-gel. Some scholars have examined the abrasion resistance of multilayer AR films, the center of which includes the sol-gel[7] and sputtering[8]. It is rare to find reports on the abrasion resistance of AR films prepared by EBE, which is the main method in preparing AR films in the coating industry. Therefore, it is necessary to examine the effect of process conditions on the abrasion resistance of broadband AR films prepared by EBE. In this letter, we focus on the effect of different temperatures, ion beam energies, and cooldown times on the abrasion resistance of broadband AR films composed of $SiO_2$and TiO_2 prepared by EBE with ion beam assistance (IBA).

Four-layer broadband AR films composed of SiO_2 and TiO_2 were grown on a one-side polishing K9 (1-mm thickness) substrate by using the EBE method with IBA (PMC90S, Protech Korea Co. Ltd). The film's band was from 620 to 860 nm, and the reflectivity was less than 0.5%. The purities of the deposited sources for SiO_2 was 99.99% and for TiO_2 was 99.99%. Before the deposition, TiO_2 was premelted in order to remove its impure gas content, which could ensure the absence of splashing and the steady rate of evaporation in the process of deposition. Firstly, the K9 substrate was cleaned by ultrasonic with acetone and alcohol, on which the lying oxidation layer was removed by hydrofluoric acid, then it was cleaned again by deionized water. Finally, the substrate was dried in nitrogen gas ambient before the deposition. The purpose was to make the multilayer uniform. The substrate was placed on a uniformly rotating (40 rpm) workpiece shelf whose distance from the evaporation source was 1.5 m. In the process of deposition, the evaporation rates of TiO_2 (0.5 nm/s) and SiO_2 (1 nm/s) were controlled accurately by a silicon crystal oscillation monitor (IC5), and an O_2^+ ion beam with high energy produced by O_2 (99.9999% purity) and an end-hall ion source assisted in the preparation.

The experiments were divided into three groups, and the seven kinds of samples were finished. The first group of samples was prepared at different temperatures, which were 200, 300, and 400 °C. The else deposition conditions were as follows: the chamber was evacuated to a base pressure of 2.2×10^{-2} Pa, the flow of O_2 was at a rate of about 30 sccm, the anode voltage of the ion source was 130 V, and the cool time after the deposition was 20 min. The second group of samples was prepared at different anode voltages of the ion source, which were 120, 130, and 140 V. The else deposition conditions were as follows: the chamber was evacuated to a base pressure of 2.2×10^{-2} Pa, the flow of O_2 was at a rate about 30 sccm, the deposition temperature was 300 °C and the

 © 2010 Chinese Optics Letters

cool time after the deposition was 20 min. The third group of samples was prepared at different cool times after the deposition, which were 20, 60, and 180 min. The else deposition conditions were as follows: the chamber was evacuated to a base pressure of 2.2×10^{-2} Pa, the flow of O_2 was at a rate of about 30 sccm, the deposition temperature was 300 °C, and the anode voltage of the ion source was 130 V.

The spectrum properties of the samples were measured by an UV-VIS-IR spectrophotometer (Lambda 950, PerkinElmer, US). At room temperature, the morphology of the AR films was characterized by atomic force microscopy (AFM) with a contact scan method (CSPM4000, Being Nano-Instruments Ltd. China), whose scan area was 8 × 8 (μm). The examination for the abrasion resistance of the AR films was carried out by a copper pen with a rubber eraser, as shown in Fig. 1, which is according to MIL-C-48497A4.5.5.1 standard. The steps in examining abrasion resistance were as follows. Firstly, the rubber eraser was vertically bound on the surface of the film. Secondly, 1.1-kg weight was loaded on the testing film surface by the rubber eraser while the red line at the end of the pen was observed. Then the same part (2–3 cm long) of the testing film surface was rubbed 20 times. Finally, the testing film surface was cleaned with alcohol and ether. After the examination, abrasion resistance was quantified by the scratch number measured by a metalloscope.

Figure 2 depicts the spectrum curve of the AR film prepared by EBE. Despite the different deposition conditions, the spectrum properties of the seven kinds of samples show no differences because these samples have the same film system structure. Hence, there is one curve drawn in Fig. 2 for a clear observation. It shows that the reflectivity of the AR film is less than 0.5% from 620 to 860 nm; further, it is nearly transparent completely from 640 to 860 nm in which the reflectivity is less than 0.2%, indicating that the spectrum properties of the samples are according to the design request, and the optical quality of all samples is good.

Fig. 1. Copper pen with rubber eraser for testing abrasion resistance.

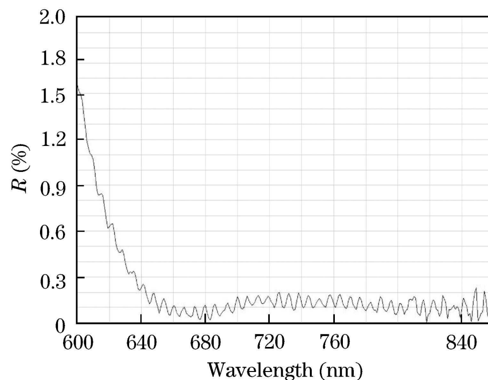

Fig. 2. Spectrum curve of the AR film.

Figures 3–5 show the morphologies of the first group of samples grown under three different temperatures. Figure 3 depicts the AFM photograph of the AR film prepared at 200 °C whose serial number is 1. Similarly, Figs. 4 and 5 respectively depict the AFM photographs of the AR films prepared at 300 °C and 400 °C whose serial numbers are 2 and 3. From Fig. 3, it can be observed clearly that there are no crystal grains appearing at the surface of sample 1 whose roughness values are 11 nm (S_a denotes the roughness average) and 16 nm (S_q denotes root mean square). However, in Fig. 4, clear triangular crystal grains can be observed, which distribute very uniformly and compactly the entire surface of sample 2 whose roughness values are 5.57 nm (S_a) and 7.78 nm

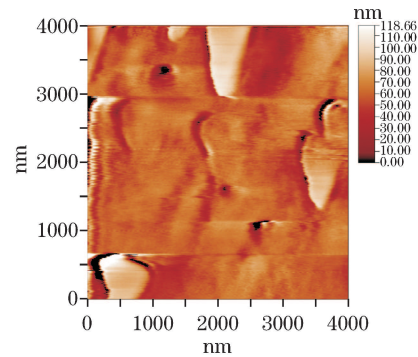

Fig. 3. AFM morphology of sample 1 prepared at 200 °C.

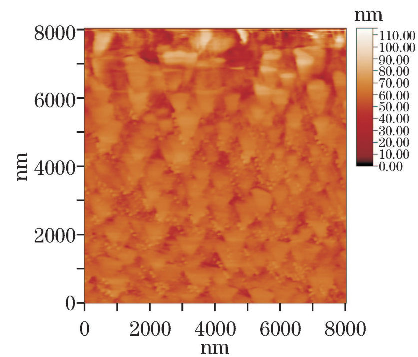

Fig. 4. AFM morphology of sample 2 prepared at 300 °C.

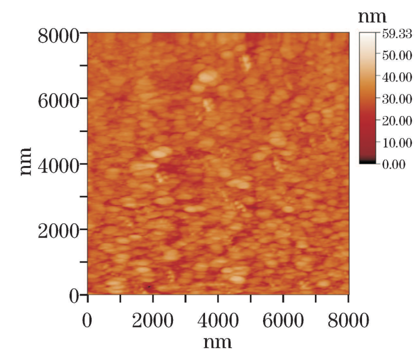

Fig. 5. AFM morphology of sample 3 prepared at 400 °C.

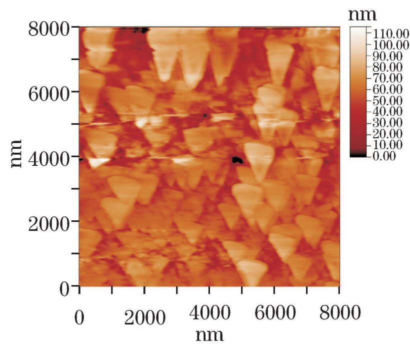

Fig. 6. AFM morphology of sample 4 prepared at 120 V of the end-hall ion source.

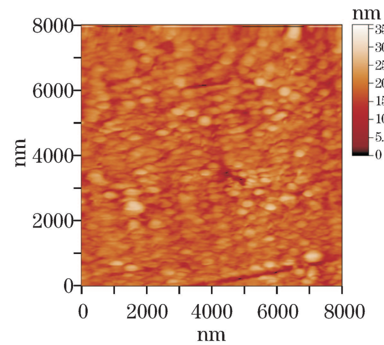

Fig. 7. AFM morphology of sample 5 prepared at 140 V of the end-hall ion source.

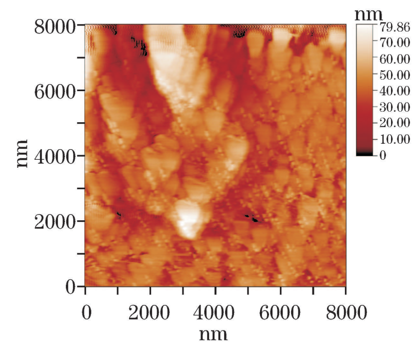

Fig. 8. AFM morphology of sample 6 prepared with 60-min cool time.

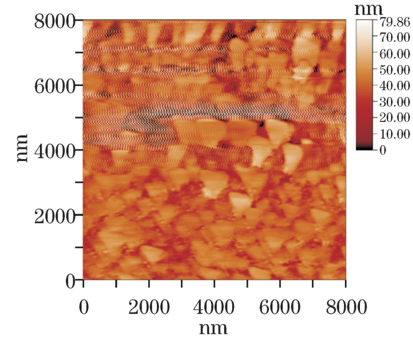

Fig. 9. AFM morphology of sample 7 prepared with 180-min cool time.

(S_q). Consequently, in Fig. 5, clear circular crystal grains can be observed, which also distribute very uniformly and compactly the entire surface of sample 3 whose roughness values are 2.9 nm (S_a) and 3.78 nm (S_q). In Figs. 3–5, it is indicated that with increasing the substrate temperature, the crystalline state of the AR film becomes more obvious. From 200 to 300 °C, the surface morphology of the film changes from amorphous to crystal with compact triangular grains. Consequently, from 300 to 400 °C, the crystal grains at the surface of the film changed from triangular to circular, which is steadier. The reason is that due to the higher surface kinetic energy with the substrate temperature, the mobility of the material molecule is increased in favor of crystallization. Furthermore, from the AFM reports, it is known that with increasing the substrate temperature, the roughness of the film surface becomes lower due to the crystalline state of the AR film. At 200 °C, the low substrate temperature leads to the low mobility of the material molecule, which cannot form compact crystal grains. As a result, the structure of the film becomes loose, and there is a mass of interspaces and gullies on the surface, leading to high roughness values. Nevertheless, at 300 °C, the surface roughness becomes low because compact triangular grains appear, and at 400 °C, the roughness becomes even lower because the grains' shape changes to round, which is smoother.

The morphologies of the second group of samples grown under three different anode voltages of the ion source are presented in Figs. 6 and 7. Figure 6 depicts the AFM photograph of the AR film prepared at 120 V whose serial number is 4. Similarly, Fig. 7 depicts the AFM photograph of the AR film prepared at 140 V whose serial number is 5. The process conditions of the sample prepared at 130 V are identical with those of sample 2, so Fig. 4 shows the AFM photograph of the AR film prepared at 130 V. In Fig. 6, clear triangular crystal grains can be observed whose sizes are in conformity and which distribute non-uniformly and arrange incompactly at the entire surface of sample 4 whose roughness values are 10.9 nm (S_a) and 14.1 nm (S_q). In Fig. 7, it can be observed clearly that there are circular crystal grains which also distribute very uniformly and compactly at the surface of sample 5 whose roughness values are 2.16 nm (S_a) and 2.89 nm (S_q) from the AFM reports. In Figs. 2, 6, and 7, it is concluded that with the anode voltage of the increasing ion source increasing, the crystalline state of the AR film becomes better. From 120 to 130 V, the crystal grains at the surface of the film became more uniform and compact. Further, the crystal grains at the surface of the film changed from triangular to circular from 130 to 140 V, which is similar to that which happened in the range of 300–400 °C. The reason is that with the anode voltage of the increasing ion source, the momenta of the material molecule transferred from the energy of the ion beam are enhanced, leading to the increased mobility of the molecule in favor of crystallization. Otherwise, it is suggested that with the energy of the increasing ion beam, the roughness of the film surface becomes lower due to the crystalline state of the AR film. At 120 V, the low energy of the ion beam, which cannot restrain the column structure growth, leads to the formation of incompact crystal grains, and there is a mass of interspaces in the film that leads to high roughness. However, at 130 V, the surface roughness becomes low because compact triangular grains appear, and at

140 V, roughness becomes lower because the grains' shape changes to round, which is smoother.

Figures 8 and 9 show the morphologes of the third group of samples grown under three different cool times after deposition. Figure 8 depicts the AFM photograph of the AR film whose serial number is 6, cooled for 60 min in the vacuum after preparation. Similarly, Fig. 9 depicts the AFM photograph of the AR film whose serial number is 7, cooled for 180 min. The process conditions of the sample cooled for 20 min are identical to those of sample 2, so Fig. 4 shows the AFM photograph of the AR film cooled for 20 min. In contrast to Figs. 4 and 8, it can be observed clearly that the crystal grains are still triangular, some of which become bigger, resulting in non-uniformity and incompactness on the surface of sample 6 whose roughness values are 8.25 nm (S_a) and 11.2 nm (S_q). Consequently, in contrast to Figs. 8 and 9, most of the triangular grains become bigger, making the uniformity and compactness worse on the surface of sample 7 whose roughness values are 9.17 nm (S_a) and 12.7 nm (S_q). Hence, in Figs. 4, 8, and 9, it is suggested that with increasing the cool time after deposition, the size of the crystal grain of the AR film becomes big, and the uniformity and compactness of the grain distribution tend to deteriorate. Owing to the high temperature of the vacuum, which needs a long time to cool, the product lying in the vacuum suffered an anneal process equivalently after deposition. Therefore, the crystal grains continued to grow with the energy from the heat of the vacuum and because of the non-uniform temperature of the vacuum due to the heater of the coater closed the size of the every grains was different greatly each other leading the uniformity and compactness of the film worse. Further, from the AFM reports, it is known that with the cool time after deposition, the increase in the roughness of the film surface becomes higher due to the deterioration in the uniformity and compactness of the film.

After the examination of abrasion resistance of the seven kinds of samples according to MIL-C-48497A4.5.5.1 standard, the detailed data are shown in Table 1. Abrasion resistance was quantified by the scratch number watched by the metalloscope, and the data denote the scratch number on every 0.01-mm^2 surface area of the film. Figure 10 shows the abrasion surface of samples 1, 2, and 3 measured by the metalloscope. From Table 1, only sample 2 shows to be a qualified product. Figure 11 depicts the relationship between abrasion resistance and the roughness of the seven kinds of samples. It can be observed clearly that with increasing the substrate temperature, the roughness of the films decreases gradually, but the abrasion resistance of which first improves then worsens due to the change in the grains' shape. The same situation occurs with increasing the in anode voltage of the ion source, but with increasing the cool time after deposition, the roughness and abrasion resistance of the films both become worse gradually. Hence, it is concluded that surface roughness is the dominant factor that influences the abrasion resistance of AR films when the roughness is relatively great. This is because that the greater the roughness, the bigger the friction coefficient, and abrasion resistance becomes worse. However, when the roughness is much lower, the change in the grains' shape becomes the dominant factor influencing abrasion resistance. The experiments prove that the abrasion resistance of the triangular crystal grains is better than that of the circular crystal grains, which is possibly due to the higher hardness of the former than the latter.

In preparing broadband AR films with good abrasion resistance using the EBE method with IBA, the main

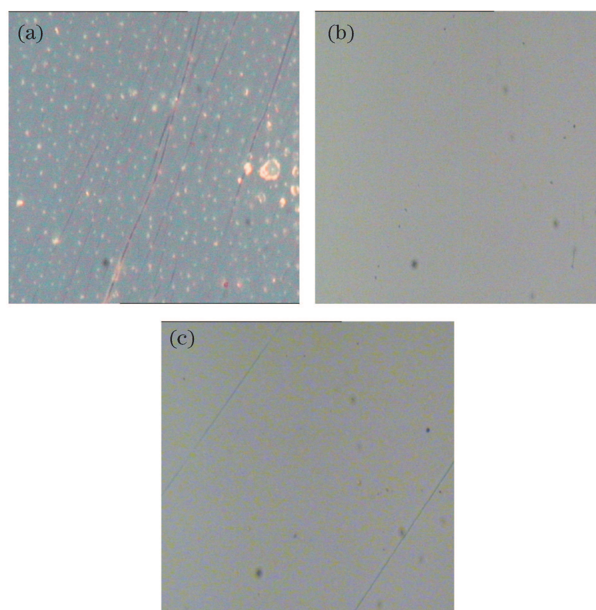

Fig. 10. Abrasion surfaces of samples (a)1, (b)2, and (c)3 observed by the metalloscope.

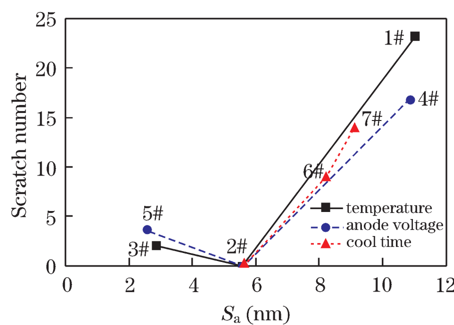

Fig. 11. Abrasion resistance curve of the roughness of seven samples.

Table 1. Abrasion Resistance of the Samples Prepared at Different Process Conditions

	Group 1 (Different Temperature)			Group 2 (Different Anode Voltage)			Group 3 (Different Cool Time)		
Sample Number	1# (200 °C)	2# (300 °C)	3# (400 °C)	4# (120 V)	2# (130 V)	5# (140 V)	2# (20 min)	6# (60 min)	7# (180 min)
Scratch Number (0.01 mm^2)	23	0	2	17	0	4	0	9	14

consideration must be the low roughness of the film surface, which means there must be uniform and compact crystal grains at the surface of the film. Hence, to achieve this goal, the temperature of the substrate should be increased at the same level as that of the ion beam, and the cool time after the deposition should be shortened so that it would not affect the shape of the substrate. At the same time, consideration must be given to the fact that the crystal grain shape will change will affect the abrasion resistance. Therefore, the roughness of the film surface should not be set to the lowest as this will result in a significant change in the crystal grain shape. The experimental results work show that the AR film with triangular grain and moderate roughness has good abrasion resistance.

References

1. D. Ma, S. Ma, K. Xu, and S. Veprek, Acta Metall. Sin. (in Chinese) **40,** 1037 (2004).
2. Y. Zhang, Y. Wu, D. Ba, and S. Ma, J. Iron Steel Res. (in Chinese) **19,** 50 (2007).
3. X. Zhang, B. Ye, S. Dai, Z. du, and P. Zhang, Lubric. Eng. (in Chinese) **179,** 82 (2006).
4. Y. Chen and W. Liu, Tribology (in Chinese) **21,** 274 (2001).
5. Y. Wang and F. Yan, J. Mater. Sci. Eng. (in Chinese) **23,** 879 (2005).
6. W. Wang, P. Sun, and G. Dai, Chinese J. Rare Metals (in Chinese) **25,** 78 (2001).
7. Y. Xu, L. Zhang, D. Wu, Y. Sun, Z. Huang, X. Jiang, X. Wei, Z. Li, B. Dong, and Z. Wu, J. Opt. Soc. Am. B **22,** 1899 (2005).
8. Y. Taga and T. Itoh, Appl. Opt. **28,** 2690 (1989).
9. T. Wang, J. Gao, X. Wang, Q. Song, H. Chen, X. Chen, Z. Shen, Z. Shan, and W. Ling, Opt. Instrum. (in Chinese) **28,** 79 (2006).
10. T. Yanagisawa, A. Nakajima, M. Sakai, Y. Kameshima, and K. Okada, Mater. Sci. Eng. B **161,** 36 (2009).